# Strongly Luminescent Tungsten Emitters with Emission Quantum Yields up to 84%: TADF and High-Efficiency Molecular Tungsten OLEDs

Kaai-Tung Chan, Tsz-Lung Lam, Daohong Yu, Lili Du, David Lee Phillips, Chun-Lam Kwong, Glenna So Ming Tong,* Gang Cheng,* and Chi-Ming Che*

**Abstract:** Metal-TADF (thermally activated delayed fluorescence) emitters hold promise in the development of next generation light-emitting materials for display and lighting applications, examples of which are, however, largely confined to $Cu^{I}$ and recently $Au^{I}$, $Ag^{I}$ and $Au^{III}$ emitters. Herein is described the design strategy for an unprecedented type of metal-TADF emitter based on inexpensive tungsten metal chelated with Schiff base ligand that exhibit high emission quantum yields of up to 56% in solutions and 84% in thin-film (5 wt% in 1,3-bis(N-carbazolyl)benzene, mCP) at room temperature. Femtosecond time-resolved emission (fs-TRE) spectroscopy and DFT calculations were undertaken to decipher the TADF properties. Solution-processed OLEDs fabricated with the W-TADF emitter demonstrated external quantum efficiency (EQE) and luminance of up to 15.56 % and 16890 cd $m^{-2}$ respectively.

In view of the low earth abundance of noble metals such as iridium, platinum and ruthenium, there is a growing interest to develop new types of luminescent metal complexes using inexpensive, earth-abundant metals for application studies.[1] In the molecular design strategies, achieving high emission quantum yield ($\Phi_{em}$) and fast radiative decay rate ($k_r$) are two important challenges to overcome as these are the key photo-physical attributes required for a metal emitter to realize practical material application. As up to now, only $Cu^{I}$-TADF[2] and a handful of $Ag^{I}$-,[3] $Au^{I}$-[4] and $Au^{III}$[5]-TADF emitters have been reported in this endeavour.[6]

Tungsten, as a third-row transition metal with much higher earth abundance with respect to noble metals and a large spin-orbit coupling (SOC) constant of 2433 $cm^{-1}$,[7] is an appealing candidate in the design of new luminescent metal materials, yet air-stable and strongly luminescent tungsten complexes were uncharted until our recent report on two classes of luminescent $W^{VI}$ *cis*-dioxido Schiff base and quinolinolate complexes.[8] These complexes exhibit $\Phi_{em}$ of up to 2.8% in dichloromethane and 22% in thin film at room temperature and were employed as dopant to fabricate the first molecular W-OLED. While the proof of principle was demonstrated, these performance data are far from threshold for practical applications. In quest of engineering air-stable $W^{VI}$ complexes with competitive luminescent properties toward efficient OLED emitters, we conceive that installing arylamino substituent(s) to the Schiff base ligand scaffold, as inspired by our recent findings on gold(III)-TADF emitters,[5] will significantly change the nature of the emissive excited states, thereby increasing the radiative decay rate constants and improving the emission quantum yields. Herein is described the first example of strongly luminescent tungsten-TADF emitter. The decently high external quantum efficiency (EQE) of the as-fabricated OLEDs highlights the prospect of W-TADF emitters as new generation of earth-abundant metal emitters with practical potential.

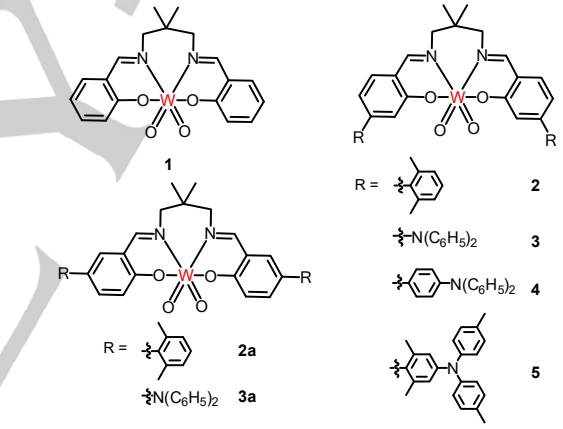


**Figure 1.** Tungsten(VI) complexes prepared in this work.

Figure 1 depicts the chemical structures of $W^{VI}$ Schiff base complexes studied in this work. The $W^{VI}$ complexes (**1**–**5**, **2a** and **3a**) were synthesized by reacting the Schiff base ligand with $[WO_2Cl_2(dme)]$ (dme = dimethoxyethane) in the presence of triethylamine in refluxing dichloromethane under inert atmosphere[9] or with $[W(eg)_3]$ (eg = 1,2-ethanediolato) in refluxing methanol open to air[10] and were isolated as air-stable yellow or orange solids in moderate to excellent yields (25–92.9 %). The experimental procedures and full characterizations of the ligands and $W^{VI}$ complexes are detailed in the Supporting Information.

All $W^{VI}$ complexes exhibit good solubility in $CH_2Cl_2$, tetrahydrofuran, toluene, but are moderately soluble in methanol, and are stable in chloroform over a week under ambient conditions. They have high thermal stability with decomposition temperature up to 363 °C as revealed by thermogravimetric analysis (Table S1; Figure S1–S3). All the $W^{VI}$ complexes feature two moderately intense IR absorptions at 928–937 $cm^{-1}$ and 887–899 $cm^{-1}$ attributed to asymmetric and symmetric stretches of the *cis*-$WO_2$ motif

[a] Dr. K.-T. Chan, Dr. T.-L. Lam, Dr. L. Du, Prof. Dr. D. L. Phillips, C. L. Kwong, Dr. G. S. M. Tong, Dr. G. Cheng, Prof. Dr. C.-M. Che
State Key Laboratory of Synthetic Chemistry
Department of Chemistry, The University of Hong Kong
Pokfulam Road, Hong Kong SAR, China.
E-mail: cmche@hku.hk; tongsm@hku.hk; ggcheng@hku.hk
[b] Dr. D. Yu, Prof. Dr. C.-M. Che
Department of Chemistry, Southern University of Science and Technology of China, Shenzhen, Guangdong, 518055, China
[c] Dr. G. Cheng, Prof. Dr. C.-M. Che
HKU Shenzhen Institute of Research and Innovation
Shenzhen, Guangdong, 518053, China

Supporting information for this article is given via a link at the end of the document.((Please delete this text if not appropriate))

respectively. The asymmetric coordination of the Schiff base ligands to a *cis*-$WO_2$ core results in four inequivalent germinal methylene proton resonances in the 2,2-dimethylpropane bridge, which appear in the AB pattern as four doublets in the range of 3.5–4.9 ppm with coupling constants of 11–12 Hz. In cyclic voltammograms (Table S2 and S3), except **2**, complexes **1**–**5** show one quasi-reversible/irreversible electrochemical oxidation at ca. 0.90–1.64 V (vs SCE) in DMF, which is attributed to ligand-centered oxidation at the Schiff base ligand. Installation of electron-donating arylamino groups in **3**–**5** engenders a considerable cathodic shift of the oxidation wave by 0.23–0.74 V with respect to **1**. The first irreversible reduction process of **1**–**5** occurs at –1.33 to –1.43 V (vs SCE). These irreversible reductions are assigned to $W^{VI}$ to $W^{V}/W^{IV}$ reduction.[9] The X-ray crystal strucutres of **2**, **3** and **5** each show a distorted octahedral molecular geometry with *cis*-β-dioxido configuration (Figure S4–S6). Notably, as induced by steric congestion, sizable dihedral angles of 60–62°between the phenolic and the 2,6-dimethylphenyl moieties were found in **5**.

The photophysical data of **1**–**5**, **2a**, and **3a** are summarized in Table 1 and Table S7. In $CH_2Cl_2$, complexes **1**–**5** display similar spectral profiles in the UV-visible absorption spectra with two intense broad absorption bands at 270–307 nm ($\varepsilon$ = 18.4–63.6×$10^3$ $mol^{-1}$ $dm^3$ $cm^{-1}$) and at 402–407 nm ($\varepsilon$ = 5.2–38.4×$10^3$ $mol^{-1}$ $dm^3$ $cm^{-1}$) respectively (Figure 2a). Both of these absorption bands are tentatively assigned to intraligand ($^1$IL) π→π* transitions of the Schiff base ligands.[7] The lowest energy absorption band for the arylamino-units-bearing complexes **3**–**5** are more intense ($\varepsilon$ = 10.6–38.4 × $10^3$ $mol^{-1}$ $dm^3$ $cm^{-1}$), compared to those of **1** and **2** ($\varepsilon$ = 5.2–5.4 × $10^3$ $mol^{-1}$ $dm^3$ $cm^{-1}$). TDDFT calculations revealed that the absorption bands at 400–410 nm are derived from the spin-allowed intraligand charge-transfer ($^1$ILCT) transition from the π orbital of the arylamino donor to the π* orbital of the Schiff base ligand with a minor contribution of ligand-to-metal charge transfer (LMCT) character (8–13% for complexes **3–5**). Intriguingly, complex **3a** displays a marked red-shift of the lowest energy absorption band by 75 nm (3880 $cm^{-1}$) relative to its positional isomer **3** (Figure S12); on the other hand, the lowest energy absorption band of the positional isomer pair, **2** and **2a**, with 2,6-dimethylphenyl substituents, display only a slight shift of 12 nm (720 $cm^{-1}$) (Figure S13). DFT calculations showed that the LUMO of **3a** is lower-lying than that of **3** (Figure S35); this is due to the fact that,

**Table 1.** Photo-physical data of $W^{VI}$ emitters.

| | Absorption | Emission | |
|---|---|---|---|
| | in $CH_2Cl_2$ | in $CH_2Cl_2$ | 5 wt% in mCP fiim |
| | $\lambda_{abs}$ [nm] ($\varepsilon$ [×$10^3$ $mol^{-1}$ $dm^3$ $cm^{-1}$])[a] | $\lambda_{em}$ [nm] ($\tau$ [μs], $\Phi_{em}$ [%], $k_r$ [$10^3$ $s^{-1}$])[a] | $\lambda_{em}$ [nm] ($\tau$ [μs], $\Phi_{em}$ [%], $k_r$ [$10^3$ $s^{-1}$][b]) |
| **1** | 270 (26.2), 299 (18.2), 402 (5.5) | 582 (83.6, 3.0, 0.4) | 471, 504, 534 (51.0,14, 2.7) |
| **2** | 307 (18.4), 403 (5.2) | 571 (76.2, 8.4, 1.1) | 578 (222.1, 28, 1.3) |
| **3** | 291 (22.8), 404 (32.9); 294 (24.5), 410 (36.0)[c] | 579 (8.0, 6.8, 8.0); 565 (28.2, 17, 6.0)[c] | 546 (252.6, 48, 1.9) |
| **4** | 297 (49.8), 407 (38.4); 299 (45.2), 410 (36.7)[c]; | 608 (4.6, 11, 23.9); 583 (22.1, 28,12.7)[c]; | 567 (227.8, 49, 2.2) |
| **5** | 304 (63.6), 405 (10.9); 300 (67.1), 400 (11.4)[d] | non-emissive; 554 (14.7, 56, 38.1)[d] | 554 (2.0[e], 84, 420.0) |
| **2a** | 250 (47.4), 302 (15.2), 415 (3.7) | 615 (79.0, 6.5, 0.8) | 602 (176.2, 21, 1.2) |
| **3a** | 295 (47.7), 479 (2.3) | 630 (1.0, 0.2, 2.0) | weak |

[a] Measurements were performed in solution at 2 × $10^{-5}$ M at 298 K. [b] Radiative decay rate. [c] Measured in $CHCl_3$. [d] Measured in toluene. [e] Weighted average lifetime $\tau_{av} = (A_1\tau_1+A_2\tau_2)/(A_1+A_2)$ for biexponential decay; $A_1$ and $A_2$ are pre-exponential factors.

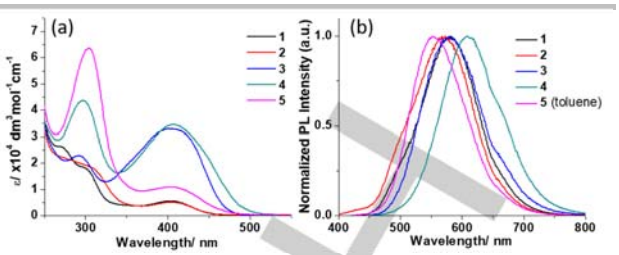


**Figure 2.** (a) UV-vis absorption and (b) emission spectra of **1**–**5** in $CH_2Cl_2$ or toluene ($\lambda_{ex}$: 400 nm) at 298 K.

in addition to the negative inductive effect exerted by the amino nitrogen in both complexes **3** and **3a** which stabilizes the LUMO, there is also a postive mesomeric effect from the -$NPh_2$ groups in **3** but not in **3a** that destabilizes the LUMO (Figure S34).

All complexes are luminescent in degassed solutions, solid states, and thin-film samples at 298 and 77K (Table 1 and Table S7). Complexes **1**–**5** display green to orange emission in degassed solutions at 298 K (Figure 2b and Figure S15–S19); the emission bands are generally broad and structureless with maxima at 537–626 nm and the emission lifetimes ($\tau$) are in the range of 0.1–117.8 μs. The emission maxima of the positional isomers **2a** and **3a** in $CH_2Cl_2$ are redshifted from **2** and **3** by 44 nm (1250 $cm^{-1}$) and 51 nm (1400 $cm^{-1}$) respectively (Figure S20 and S21).The emission profiles of **1** and **2** are relatively insensitive to solvent polarity ($\Delta\lambda_{max}$ < 7 nm), similar to the previously reported $W^{VI}$ Schiff base complexes with a $^3$IL emissive excited state.[8] In contrast, those arylamino-substituents-bearing analogues, **3**–**5**, exhibit significant solvatochromic shift with $\Delta\lambda_{max}$ spanning the range of 51–98 nm. The Lippert–Mataga plots of **3**–**5** display large positive slopes of ~11190–13200 $cm^{-1}$ (Figure S22–S24), suggesting a large change in dipole moment upon attaining the emissive excited state which substantiates an emissive excited state of strong charge-transfer character. *Strikingly, the emission quantum yields ($\Phi_{em}$) of **3**–**5** in solutions are up to 17–56%, which are ca. 2- to 20-fold higher than those of **1** (3.0%), **2** (8.4%) and the reported $W^{VI}$ Schiff base emitters (up to 2.8%).*[8] From the excited state decay rates in Table 1 and Table S7, the enhanced radiative decay rates ($k_r$) for **5** ($10^4$ $s^{-1}$), underlie its superior $\Phi_{em}$ with respect to **1**–**4** and the reported $W^{VI}$ counterparts ($k_r$ = $10^2$–$10^3$ $s^{-1}$) in toluene,[8] as their non-radiative decay rates ($k_{nr}$) are all of similar order of ($k_{nr}$ ~ $10^4$ $s^{-1}$; Table S7). In mCP thin films doped with 5 wt% W complexes, the arylamino-substituents-bearing complexes, likewise, reveal a much higher $\Phi_{em}$, with the $\Phi_{em}$ of **3** and **4** being close to 50% and that of **5** topping out at 84%, compared to **1** (22%) and **2** (28%). More importantly, in addition to the high $\Phi_{em}$, *the emission lifetime of **5** in the doped-film is only 2.0 μs, which is much shorter than its counterparts **1**–**4** (51.0–252.6 μs); the combined high emission quantum yield and short emssion lifetime give rise to large $k_r$ value of 4.2×$10^5$ $s^{-1}$ for **5**.*

Large $k_r$ values on the order of $10^5$–$10^6$ $s^{-1}$ are usually bound to $Ir^{III}$, $Pt^{II}$, and $Os^{II}$ complexes where the emissive excited states have substantial metal character, such as the $^3$MLCT excited state, and the metal ions have large SOC constants.[11] In the present study, because the hexavalent $W^{VI}$ ion has a $d^0$ electronic configuration, there cannot be any low-lying $^3$MLCT excited state. Thus, the much accelarated $k_r$ of **5** in both toluene solution and doped-film at room tempearature is intriguing, particularly when **5** closely resembles **4** where the two differ mainly by a pair of *ortho*-methyl groups on the triphenylamine (TPA) moieties; the $k_r$ values of **5** are more than 100-

fold greater than those of **4** in both solution and film states, suggesting that **5** emits with a mechanism distinct from that of **4**. Given the fact that (1) the emissive excited state is mainly of charge-transfer character as reflected from the broad emission band and large solvatochromism, (2) a slight red-shift of 7 nm in emission of mCP film of **5** from 298 K to 77 K accompanied by a surge of emission lifetime to 358.0 $\mu s$, similar to those of **1**–**4** at RT, was observed (Figure S25) and, (3) the presence of methyl groups on TPA units in **5** mainly controls the dihedral angle between the TPA donor and the Schiff base ligand, and hence the spatial separation between the donor and acceptor orbitals in which case the energy gap between the respective $^{1,3}$ILCT excited states may be much smaller in **5** than **4**, it is proposed that the emission mechanism of **5** is thermally activated delayed fluorescence (TADF). The findings from femtosecond time-resolved fluorescence (fs-TRF) measurements of **5** lend support to this proposition. As the fs-TRF spectra represent $S_1 \rightarrow S_0$ prompt fluorescence (PF), the similarity of the emission profile between the fs-TRF (Figure 3a) and steady-state emission spectra ($\lambda_{max} \approx 560$ nm) suggest that both are derived from $S_1 \rightarrow S_0$ radiative decay with the latter being a delayed fluorescence. The intersystem crossing (ISC) time contant of **5** for the $S_1$ to $T_n$ transition is 312 ps from the kinetic decay of PF (Figure 3b). For comparision, the steady-state emission spectrum of **1** has a significant redshift of ca. 50 nm from its fs-TRF spectra (582 vs 534 nm) (Figure S32), and hence the steady-state emission of **1** is phosphorescence.

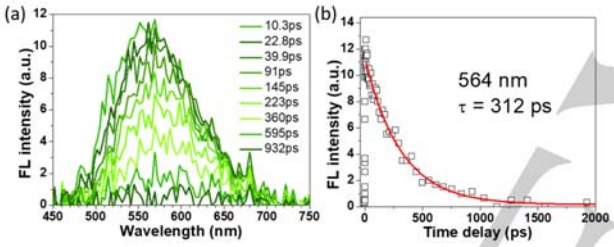


**Figure 3.** (a) Temporal evolution and (b) intensity decay profiles of fs-TRF for **5** in toluene upon photoexcitation at 400 nm.

DFT calculations were carried out for **4** and **5** to investigate the dramatic difference in $k_r$ and the possibility of TADF. The optimized ground state structures of both complexes are similar, with major difference lies on the dihedral angle ($\delta$) between the phenyl rings of the Schiff base and the TPA fragments: $\delta$ = 36–38° for **4** and 70–74° for **5** (Figure S38). This geometry difference leads to modifications of the MO surfaces and very different photo-physical properties of the two complexes. The singlet and triplet excited states were computed at the optimized ground state geometries. The lowest singlet ($S_1$) and triplet ($T_1$) excited states for both complexes are ILCT excited states, as reflected from the charge density difference (CDD) maps and the associated natural transition orbitals (NTOs) in Figure 4 and Figure S39–S40 respectively. The NTO pair, highest occupied NTO (HONTO) and lowest unoccupied NTO (LUNTO), contributes dominantly to the $S_1$ and $T_1$ excited states (eigenvalue $\nu > 0.96$). It is noted that the NTO pair is more delocalized in **4** than in **5** due to the smaller dihedral angle $\delta$ in the former than the latter. As such, there are better overlaps between the occupied and unoccupied orbitals and larger oscillator strengths for the $S_0 \rightarrow S_1$ transition in **4** than in **5**, which is in good agreement with the spectral intensities of the lowest absorption band in the UV-vis spectra of the two complexes, lending support to the reliability of the present calculations. On the other hand,

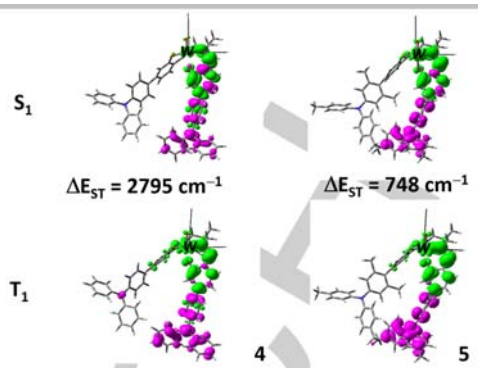


**Figure 4.** Charge density difference (CDD) maps of and energy separation between $S_1$ and $T_1$ excited states of **4** and **5** at their respective optimized $S_0$ geometries. Colour code: magenta, decrease in electron density; green, increase in electron density.

due to the smaller orbital overlap in **5**, the energy difference between $S_1$ and $T_1$ excited states ($\Delta E_{ST} = E(S_1)–E(T_1)$) are smaller in **5** ($\Delta E_{ST}$ = 2795 $cm^{-1}$ for **4** and 748 $cm^{-1}$ for **5**). Such a small $\Delta E_{ST}$ suggests favorable ISC and reverse ISC (RISC); the fast $k_r$ in **5** is thus likely derived from TADF. To give further theoretical support that the emission of **5** in toluene is derived from TADF, the singlet and triplet excited state geometries of **4** and **5** have also been optimized. At their optimized $^1$ILCT geometry, $\delta$ = 37–42° and 77–81° for **4** and **5** respectively with the computed $\Delta E_{ST}$ being more than 3000 $cm^{-1}$ for **4** but only ~1000 $cm^{-1}$ for **5**; the corresponding calculated radiative decay rate constants, $k_r^P(T_1 \rightarrow S_0)$ and $k_r^F(S_1 \rightarrow S_0)$ transitions are respectively $8.63\times10^2$ and $3.13\times10^8$ $s^{-1}$ for **4** and $2.62\times10^1$ and $3.27\times10^7$ $s^{-1}$ for **5**. Assuming fast thermal equilibrium between the $S_1$ and $T_1$ excited states (i.e. $^{1,3}$ILCT excited states), due to the large $S_1$–$T_1$ energy gap of > 3000 $cm^{-1}$, TADF is inefficient in **4** and its emission is principally phosphorescence; the calculated $k_r^P$ is also of the same order as the experimentally determined one, $k_r \approx 10^2\ s^{-1}$. On the contrary, for complex **5**, the moderate $\Delta E_{ST}$ of 1000 $cm^{-1}$ allows efficient TADF and the calculated $k_{r,avg}$ would be $5.79\times10^4$ $s^{-1}$ at rt (Figure S41). The good agreement between the computed $k_{r,avg}$ and the experimental $k_r$ of $3.81\times10^4$ $s^{-1}$ gives support that the emission mechanism of **5** in toluene involves TADF.

To investigate the impact of different emission mechanism of $W^{VI}$ complexes upon their electroluminescent (EL) properties, **4** (phosphorescence) and **5** (TADF) were respectively used as emitting dopant in solution-processed OLEDs. The device structure was ITO/PEDOT:PSS/PVK: OXD-7: W emitter/TPBi/LiF/Al for both **4** and **5**. The mixture of PVK (polyvinylcarbazole) and OXD-7 [(1,3-bis[(4-*tert*-butylphenyl)-1,3,4-oxadiazolyl]phenylene)] with a weight ratio of 9:1 was used as the host[12] and the dopant concentration was ranged from 10 to 40 wt% for both emitters. TPBi [2,2',2"-(1,3,5-benzinetriyl)-tris(1-phenyl-1-H-benzimidazole)] was used as an electron-transporting layer. As depicted in Figure S42a and S42b, with increasing concentration from 10 to 40 wt%, the EL spectra of both **4** and **5** devices slightly red-shifted by about 10 nm attributable to the increased intermolecular interactions. Compared to those of the **5** devices, the host emission originated from PVK appears more frequently in the EL spectra of **4** devices due to the much longer emission lifetime of the latter. With increasing luminance from 13 to 1500 cd $m^{-2}$ (Figure S43a), the PVK emission increased in the **4** device with 40 wt% dopant concentration because the saturation of

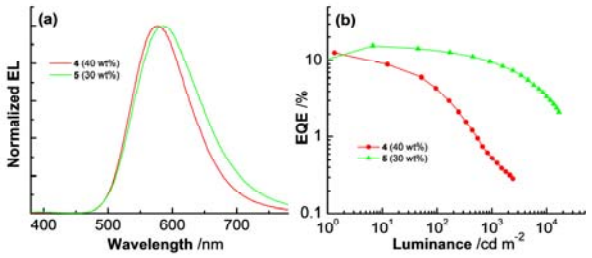


**Figure 5.** (a) EL spectra and (b) EQE-luminance characteristics of solution-processed OLEDs using **4** and **5** as emitting dopants with optimized concentration.

the excited states of **4** at high luminance blocks the energy transfer from PVK to **4** due to the long emission lifetime (227.8 μs) of **4**.[13] Onthe other hand, the PVK emission appears at very high luminance of almost 10000 cd $m^{-2}$ in the **5** device with 30 wt% dopant (Figure S43b) concentration attributed to the shorter emission lifetime (2.0 μs) of **5**. For the same reason, the efficiency roll-off is quite pronounced in the **4** devices as depicted in Figure S42c. For instance, the maximum value of EQE for the **4** device with 40 wt% dopant concentration is 12.71% while this value dramatically drops to 0.53% at a high luminance of 1000 cd $m^{-2}$, corresponding to a roll-off of 95.8%. On the other hand, the efficiency roll-off of the **5** device with 30 wt% dopant concentration (Figure 5b) was found to be highly improved, being 37.66% at 1000 cd $m^{-2}$ attributed to the shorter emission lifetime caused by the TADF mechanism of **5**. The EQE-luminance characteristics of the devices with **4** and **5** are depicted in Figure S42c and S42d, respectively, while the key EL properties of these devices are listed in Table S8. The EQE value of the **5** devices was relatively insensitive to the dopant concentration; with increasing concentration from 10 to 40 wt%, the maximum EQE ranged between 13.67 and 15.56%, revealing that the concentration quenching effect is quite weak in solution-processed OLEDs based on **5**. The EQE value of 15.56% achieved in the **5** device with 30 wt% dopant concentration represents a more than 3.2-fold improvement compared to the value of 4.79% in our previous report on the electroluminescence of W complexes.[7] Thanks to the short emission lifetime of **5**, its EQE (9.70%) at a high luminance of 1000 cd $m^{-2}$ and maximum luminance (16890 cd $m^{-2}$) are both more than 10-fold higher than those (0.73% and 1400 cd $m^{-2}$) of our reported W-OLED.[8] The performances of the TADF **5** device are approaching those of the best solution-processed metal TADF OLEDs with $Au^{I}$, $Au^{III}$, and $Cu^{I}$ complexes, whose EQEs are up to 27.5%, 23.8% and 23.0%, respectively.[4b,5,14]

In summary, this work has demostrated a molecular design approach, by incorporating strong arylamino donor groups into the ligand scaffold, to increase the radiative decay rates and boost the emission quantum yields of $W^{VI}$ Schiff base complexes. Importantly, a subtle control over the twisted angle between the arylamino donor unit and the phenolic moiety was identified to be the key to influence the excited state dynamics and realize TADF via modulating the singlet-triplet energy separation as corroborated by DFT calculations. High-efficiency solution-processed OLEDs with EQE up to 15.56% were fabricated with the W-TADF emitter. We envison that engineering tungsten complexes with TADF properties is a promising direction to develop a new class of low-cost light-emitting materials having practical interest that coud potentially rival the precious metal-based phosphor materials.

## Acknowledgements

This work is supported by Innovation and Technology Commission (HKSAR, China) to the State Key Laboratory of Synthetic Chemistry, Innovation and Technology Fund (ITF-Tier 3, ITS/140/16) administered by the Innovation and Technology Commission, General Research Fund (HKU 17330416) from Research Grants Council, Area of Excellence Scheme (AoE/P-03/08), National Key Basic Research Development Scheme (2013CB834800) and Shenzhen Basic Research Program (JCYJ20170307104939529). We thank Dr. Kam-Hung Low for assistance in solving the X-ray crystal structures of $W^{VI}$ complexes.

**Keywords:** Tungsten • Organic light-emitting devices (OLEDs) • Thermally activated delayed fluorescence (TADF)

[1] a) C. Bizzarri, E. Spuling, D. M. Knoll, D. Volz, S. Bräse, *Coord. Chem. Rev.* **2018**, *373*, 49-82; b) O. S. Wenger, *J. Am. Chem. Soc.* **2018**, *140*, 13522-13533.

[2] a) R. Czerwieniec, M. J. Leitl, H. H. H. Homeier, H. Yersin, *Coord. Chem. Rev.* **2016**, *325*, 2-28. b) R. Hamze, J. L. Peltier, D. Sylvinson, M. Jung, J. Cardenas, R. Haiges, M. Soleilhavoup, R. Jazzar, P. I. Djurovich, G. Betrand, M. E. Thompson, *Science* **2019**, *363*, 601-606; c) S. Shi, M. C. Jung, C. Coburn, A. Tadle, D. Sylvinson M. R., P. I. Djurovich, S. R. Forrest, M. E. Thompson, *J. Am. Chem. Soc.* **2019**, *141*, 3576-3588.

[3] a) M. Z. Shafikov, A. F. Suleymanova, R. Czerwieniec, H. Yersin, *Chem. Mater.* **2017**, *29*, 1708-1715; b) M. Z. Shafikov, A. F. Suleymanova, R. Czerwieniec, H. Yersin, *Inorg. Chem.* **2017**, *56*, 13274-13285.

[4] a) M. Osawa, I. Kawano, R. Ishii, S. Igawa, M. Hashimoto, M. Hoshinoa, *J. Mater. Chem. C* **2013**, *1*, 4375-4383; b) D. Di, A. S. Romanov, L. Yang, J. M. Richter, J. P. H. Rivett, S. Jones, T. H. Thomas, M. A. Jalebi, R. H. Friend, M. Linnolahti, M. Bochmann, D. Credgington, *Science* **2017**, *356*, 159-163.

[5] W.-P. To, D. Zhou, G. S. M. Tong, G. Cheng, C. Yang, C.-M. Che, *Angew Chem.* **2017**, *129*, 14224-14229; *Angew. Chem. Int. Ed*. **2017**, *56*, 14036-14041.

[6] *Highly Efficient OLEDs: Materials Based on Thermally Activated Delayed Fluorescence*, Wiley VCH, Germany, **2019**.

[7] M. Montalti, A. Credi, L. Prodi, M. T. Gandolfi, *Handbook of Photochemistry, 3rd edn*, CRC press, USA, **2006**, pp. 619-623.

[8] K.-T. Yeung, W.-P. To, C. Sun, G. Cheng, C. Ma, G. S. M. Tong, C. Yang, C.-M. Che, *Angew. Chem.* **2017**, *129*, 139-143; *Angew. Chem. Int. Ed*. **2017**, *56*, 133-137.

[9] a) Y.-L. Wong, Y. Yan, E. S. H. Chan, Q. Yang, T. C. W. Mak, D. K. P. Ng, *J. Chem. Soc., Dalton Trans.* **1998**, 3057-3064; b) Y.-L. Wong, J.-F. Ma, W.-F. Law, Y. Yan, W. T. Wong, Z.-Y. Zhang, T. C. W. Mak, D. K. P. Ng, *Eur. J. Inorg. Chem.* **1999**, 313-321.

[10] a) A. Lehtonen, *Inorg. Chem. Commun.* **2005**, *8*, 122-124; b) A. Lehtonen, *Polyhedron* **2006**, *25*, 767-775.

[11] a) Y. Chi, P.-T. Chou, *Chem Soc. Rev.* **2010**, *39*, 638-655; b) K. Li, G. S. M. Tong, Q. Wan, G. Chang, W.-Y. Tong, W.-H. Ang, W.-L. Kwong, C.-M. Che, *Chem. Sci.* **2016**, *7*, 1653-1673.

[12] G. Cheng, P.-K. Chow, S. C. F. Kui, C.-C. Kwok, C.-M. Che, *Adv. Mater.* **2013**, *25*, 6765-6770.

[13] G. Cheng, K. T. Chan, W.-P. To, C.-M. Che, *Adv. Mater.* **2014**, *26*, 2540-2546.

[14] D. Volz, Y. Chen, M. Wallesch, R. Liu, C. Fléchon, D. M. Zink, J. Friedrichs, H. Flügge, R. Steininger, J. Göttlicher, C. Heske, L. Weinhardt, S. Bräse, F. So, T. Baumann, *Adv. Mater.* **2015**, *27*, 2538–2543.

# COMMUNICATION

**A light-bulb moment of tungsten(VI) complexes:**

Incorporation of arylamino substituents into the ligand scaffold leads to the realization of the first $W^{VI}$ Schiff base complex with TADF properties which shows $\Phi_{em}$ of 56% in solution and 84% in thin film at room temperature. High-efficiency solution-processed W-OLEDs were fabricated exhibiting maximum EQE and luminance up to 15.56% and 16890 cd $m^{-2}$

.

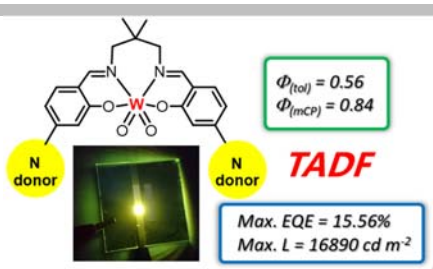


*Kaai-Tung Chan, Tsz-Lung Lam, Daohong Yu, Lili Du, David Lee Phillips, Chun-Lam Kwong, Glenna So Ming Tong,* Gang Cheng,* and Chi-Ming Che**

***Page No. – Page No.***

**Strongly Luminescent Tungsten Emitters with Emission Quantum Yields up to 84%: TADF and High-Efficiency Molecular Tungsten OLEDs**